Skyrmion-based high-frequency signal generator

Cite as: Appl. Phys. Lett. **110**, 112402 (2017); https://doi.org/10.1063/1.4978510
Submitted: 17 December 2016 • Accepted: 21 February 2017 • Published Online: 14 March 2017

Shijiang Luo, Yue Zhang, Maokang Shen, et al.

Skyrmion-based high-frequency signal generator

Shijiang Luo, Yue Zhang,[a] Maokang Shen, Jun Ou-Yang, Baiqian Yan, Xiaofei Yang, Shi Chen, Benpeng Zhu, and Long You
School of Optical and Electronic Information, Huazhong University of Science and Technology, Wuhan 430074, People's Republic of China

(Received 17 December 2016; accepted 21 February 2017; published online 14 March 2017)

Many concepts for skyrmion-based devices have been proposed, and most of their possible applications are based on the motion of skyrmions driven by a dc current in an area with a constricted geometry. However, skyrmion motion driven by a pulsed current has not been investigated so far. In this work, we propose a skyrmion-based high-frequency signal generator based on the pulsed-current-driven circular motion of skyrmions in a square-shaped film by micromagnetic simulation. The results indicate that skyrmions can move in a closed curve with central symmetry. The trajectory and cycle period can be adjusted by tuning the size of the film, the current density, the Dzyaloshinskii–Moriya interaction constant, and the local in-plane magnetic anisotropy. The period can be tuned from several nanoseconds to tens of nanoseconds, which offers the possibility to prepare high-frequency signal generator based on skyrmions. *Published by AIP Publishing.*
[http://dx.doi.org/10.1063/1.4978510]

Since it was observed in chiral magnets and thin films,[1–4] a magnetic skyrmion has received considerable attention owing to its small size, low current density for its current-driven motion, and topologically protected stability.[5–9] All these characteristics make skyrmions have significant potential to be applied to the next generation of magnetic memory devices. Many concepts for skyrmion-based devices have been proposed, such as skyrmion-based transistors,[10] logic gates,[11] and the spin-transfer nano-oscillators (STNOs).[12]

Until now, the application of skyrmions is mainly based on the motion of skyrmions driven by a dc current with spin orbit torque (SOT). Jiang *et al*. experimentally demonstrated the generation and SOT-driven motion of magnetic skyrmion bubbles from chiral stripe domains.[13] Theoretically, the SOT-driven motion of skyrmions is expressed using the Thiele equation[5,14]

$$\vec{G} \times \vec{v} + \alpha \vec{\vec{D}} \cdot \vec{v} + \vec{F}_{\text{spin}} + \vec{F} = 0, \tag{1}$$

where the first term represents the Magnus force. $\boldsymbol{G}$ is the so-called gyrocoupling vector, $\boldsymbol{v}$ is the drift velocity of the skyrmion, α is the Gilbert damping coefficient, $\vec{\vec{D}}$ is the dissipative tensor, $\boldsymbol{F}_{\text{spin}}$ is the SOT driving force acting on the skyrmion, and $\boldsymbol{F}$ is the force from boundaries, defects, and so on.

In an infinite film without any boundary or defect, a skyrmion is driven to move along a straight line at an angle with respect to the direction of the current because of the Magnus force.[15] This behavior is referred to as the skyrmion Hall effect[7] which was theoretically predicted by Zang[16] and was experimentally observed by Jiang.[17] Under the action of both the Magnus force and the $\boldsymbol{F}$, a skyrmion is driven to move along a strip-shaped nanotrack[5,18,19] or along complicated trajectories[20] or around areas with strong potential barriers.[21] In particular, Zhang *et al*. proposed a skyrmion-based STNO using the circular motion of a skyrmion in a round-shaped nanodisk.[12]

All the above investigations are based on the motion of skyrmions driven by a *dc* current. In the present work, through micromagnetic simulation, we found the high-frequency circular motion of skyrmions driven by a *pulsed* current in a *square-shaped* thin film, which may be developed as a skyrmion-based high-frequency signal generator.

A schematic of the structure and function of the skyrmion-based high-frequency signal generator is depicted in Fig. 1. The position of a skyrmion was depicted by a planar rectangular coordinate system with its origin at the film center. First, a skyrmion is created at a designated position on the diagonal of the square film by a local spin-polarized current, which is experimentally realized using a spin-polarized scanning tunneling microscope (SP-STM).[22] Then, the skyrmion is driven to move circularly along a closed curve by a pulsed current and is detected using a magnetic tunnel junction (MTJ), which is composed of a bottom ferromagnetic (FM) layer such as Co, an insulating layer, and an upper perpendicularly magnetized FM layer. When a skyrmion enters the region of MTJ, the variation of the angle of the moments in both FM layers leads to an output signal due to the tunneling magnetoresistance effect.

Our work was performed by micromagnetic simulation using the Object-Oriented MicroMagnetic Framework (OOMMF) software that contains the code for the interfacial Dzyaloshinskii–Moriya interaction (DMI).[23] A square-shaped Co/Pt bilayer with perpendicular magnetic anisotropy (PMA) was considered as the medium. In experiments, Co/Pt multilayers with alternative Co and Pt layers are usually exploited. However, it is simplified to one layer of Co since magnetic parameters but not the detailed structure of Co-Pt system matter in simulation. A 2-dimensional (2D) model with only one cell in the thickness direction was adopted since the film thickness is much smaller than its length. The area of the 2D FM layer varies from $80\,\text{nm} \times 80\,\text{nm}$ to $140\,\text{nm} \times 140\,\text{nm}$ with cell dimensions of $1\,\text{nm} \times 1\,\text{nm}$. The saturation magnetization

[a]Author to whom correspondence should be addressed. Electronic mail: Yue-Zhang@hust.edu.cn

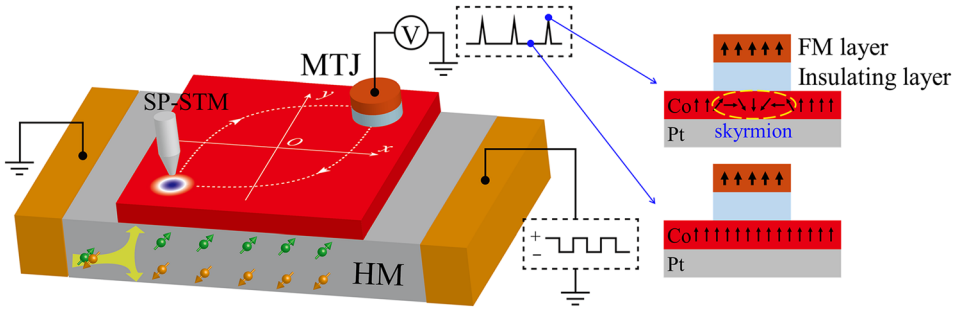

FIG. 1. Schematic of the structure and function of the skyrmion-based high-frequency signal generator. The skyrmion is driven to move circularly by a pulsed current and is detected using a MTJ.

(M_S), exchange stiffness constant (A), spin Hall angle (θ_{SH}), and damping coefficient (α) are 5.8×10^5 A/m, 1.5×10^{-11} J/m, 0.08, and 0.3, respectively.[5,24] The DMI constant (D) varies from 1.8 mJ/m^2 to 3.4 mJ/m^2. In experiments, the D larger than 2 mJ/m^2 has not been reported in the Co/Pt bilayer fabricated by sputtering. However, Yang *et al.* predicted a larger D (around 3 mJ/m^2) in a Co/Pt bilayer with 3 atomic layers of Co and good atomic-coupling at the Co/Pt interface.[25] Since D of Co/Pt bilayer is inversely proportional to the thickness of Co,[25] the D varying from 1.8 mJ/m^2 to 3.4 mJ/m^2 corresponds to the thickness of Co that is between 0.6 nm and 1 nm. It is possible to tune the magnetic anisotropy constant (K_u) of Co/Pt in a wide range by manipulating the thickness of Co and fabrication conditions. To ensure the creation and motion of a skyrmion in the simulation, the K_u is between 0.5×10^6 J/m^3 and 0.8×10^6 J/m^3. Finally, the OOMMF code assumes that the temperature is 0 K. This assumption is reasonable since the Curie temperature of Co is higher than 1000 °C, far above room temperature. Therefore, when the device is working at room temperature, the deviation from the property at 0 K due to thermal fluctuation may be small.[26]

As a representative example, we investigated the generation and motion of skyrmions driven by dc and pulsed currents and their detection by MTJ in a film with dimensions of 100 nm × 100 nm and $D = 3$ mJ/m^2, $K_u = 0.8 \times 10^6$ J/m^3. The skyrmion was first generated at the lower-left corner ($\boldsymbol{R}$, the central position of the skyrmion, is (−30 nm, −30 nm)) using a spin-polarized current with $J = 5 \times 10^{14}$ A/m^2 and spin polarization of 0.4. Then, the skyrmion was driven to move by applying a dc current in the $+x$ direction with a current density (J_d) of 2.5×10^{11} A/m^2 in the HM layer. The trajectory of the skyrmion is shown in Fig. 2(a). The dots represent the central point of the skyrmion, and the time interval between two dots is 0.1 ns. The evolution of the velocity ($\boldsymbol{v}$) using a positive dc current is shown in Fig. 2(b), where $\vec{v} = \dot{\vec{R}}(x(t), y(t))$ and "." denotes the time derivative. The skyrmion starts to move right owing to the SOT and simultaneously and rapidly deviates upward because of the repulsive force from the lower boundary and Magnus force. When crossing the diagonal, the SOT continues to drive the skyrmion to move right, but strong repulsive forces from the upper and right edges push the skyrmion to move back until

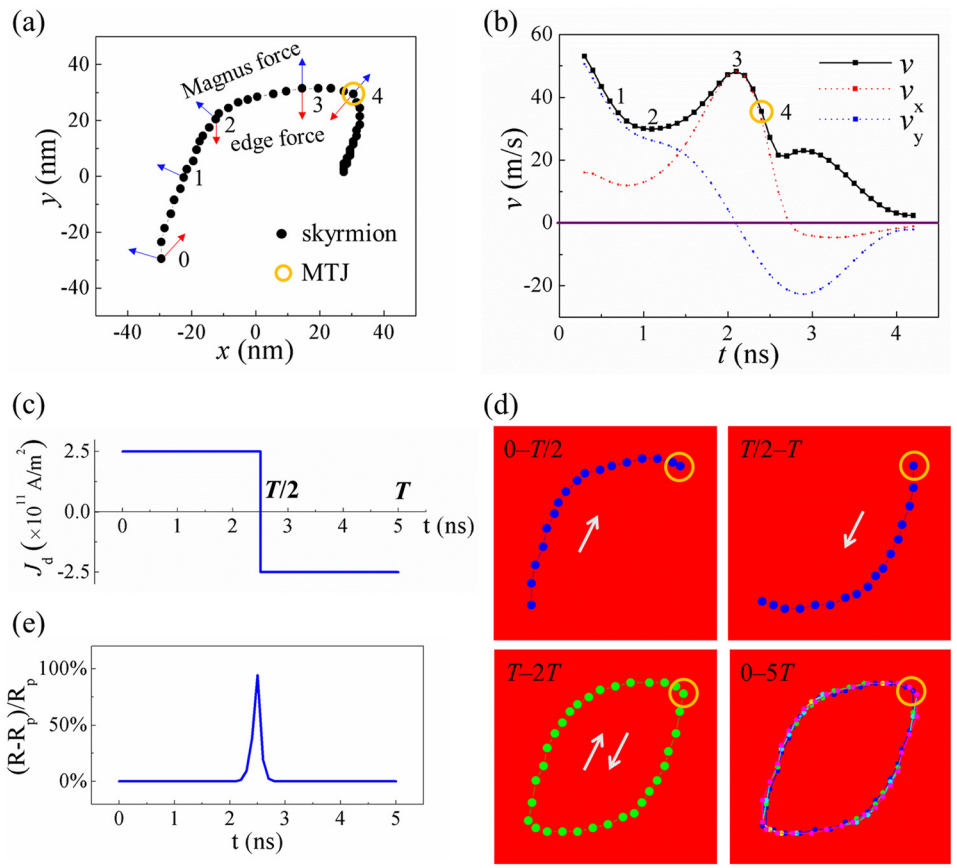

FIG. 2. (a) The trajectory of a skyrmion driven by a dc current in a square-shaped film. (b) The evolution of the drift velocity of the skyrmion. (c) The representative pulse current with a current density (J_d) of 2.5×10^{11} A/m^2 in a period (T). (d) The trajectories for the circular motion of a skyrmion using a pulsed current shown in (c) in the first half-period (0-T/2), the second half-period (T/2-T), the second period (T-2T), and the five periods from the beginning (0–5T). The orange circle at the upper-right corner indicates the position of MTJ. (e) The output resistance variation of the MTJ in the first T. R_p means the resistance of MTJ when the moment in the free layer is parallel to that in the pinned layer.

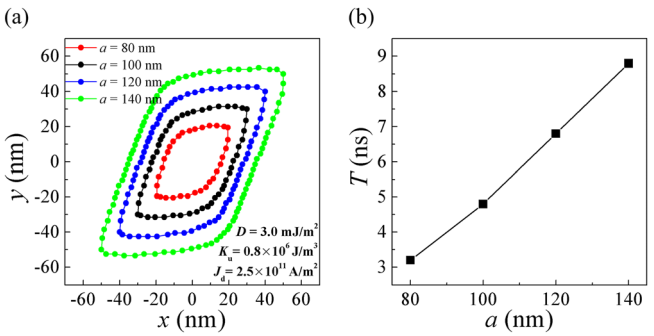

FIG. 3. (a) The trajectories for the circular motion of skyrmions in films with different lengths a. The current density J_d, magnetic anisotropy constant K_u, and DMI constant D are 2.5×10^{11} A/m^2, 0.8×10^6 J/m^3, and 3.0 mJ/m^2, respectively. (b) The period T of the circular motion as a function of a.

all the forces are totally canceled, resulting in the final stoppage.

The circular motion of a skyrmion using a pulsed current with $J_d = 2.5\times10^{11}$ A/m^2 and period (T) = 5 ns (Fig. 2(c)) in the square-shaped film is shown in Fig. 2(d). In the first half-period, the skyrmion moves from the lower-left corner to the upper-right one on the diagonal. In particular, the ending point at the end of the half-period is centrosymmetric with respect to the starting point. According to symmetry, in the subsequent half-period with $J_d = -2.5\times10^{11}$ A/m^2, the trajectory is also centrosymmetric with respect to that in the first half-period. Therefore, the skyrmion can move back to its starting point, completing a cycle. Reversing the current direction again, the skyrmion continues to move for the second cycle. The trajectories of the first five cycles overlap well. It is noted that the small inertia of the skyrmion is negligible.[12,27] Therefore, the difference in the velocity between the starting and ending points on the diagonal has little impact on the symmetry for the trajectories in the first and second current periods. As depicted in Fig. 2(e), the skyrmion was electrically detected from the variation of resistance of MTJ whose area is assumed to be identical to that of skyrmion. The tunnelling magnetoresistance, defined as $(R_{ap}-R_p)/R_p$, where R_p and R_{ap} are the resistances when the moment in the free layer is parallel to and antiparallel to that in the pinned layer, is assumed to be 100%.[28] Based on these assumptions, the resistance variation with respect to R_p when a skyrmion enters the MTJ region reaches 94%, which is derived in the supplementary material (S1).

We then investigated how the motion of a skyrmion is affected by tuning a (the length of the film), J_d, K_u, and D. First, the changes in T with a were studied. The trajectories for skyrmions in films with different a are shown in Fig. 3(a). J_d, K_u, and D are 2.5×10^{11} A/m^2, 0.8×10^6 J/m^3, and 3 mJ/m^2, respectively. The distances between the starting points and the edge are fixed at 20 nm. One can see that the

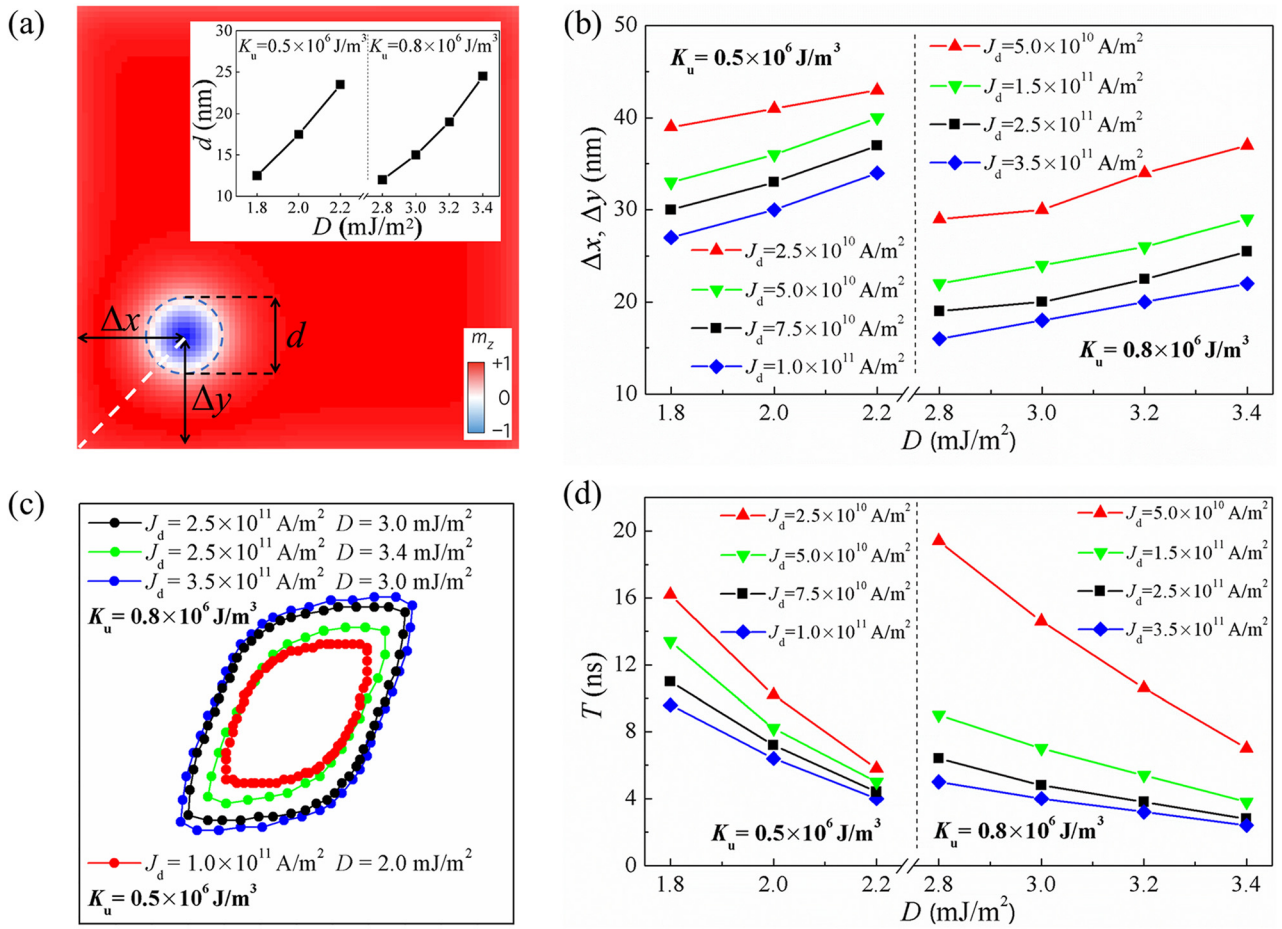

FIG. 4. (a) Δx and Δy are defined as the distances from the core of skyrmion on the diagonal to the left or right boundary and to the lower or upper boundary, respectively, and d is defined as the diameter of the circle of $m_z = 0$. The inset shows d as a function of K_u and D. (b) The dependencies of J_d, K_u, and D on Δx and Δy. (c) The representative trajectories for the circular motion of skyrmions for different J_d, K_u, and D. The dimensions of the films are 100 nm × 100 nm. (d) The dependencies of J_d, K_u, and D on the period T.

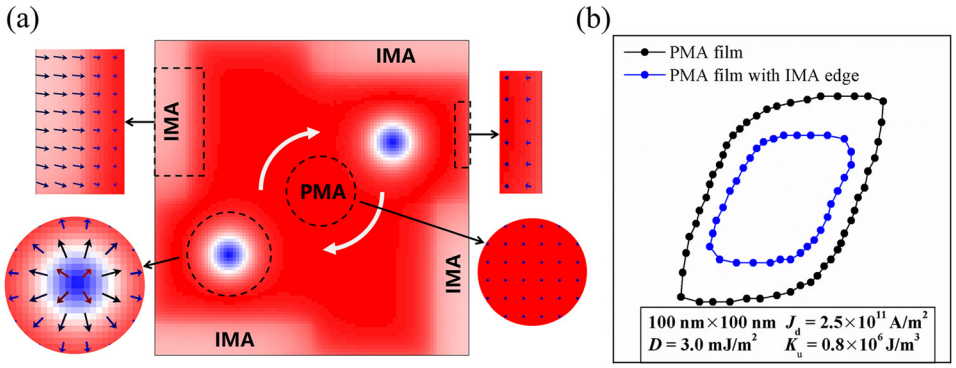

FIG. 5. (a) The composite structure consisting of a square film with PMA center areas and IMA edges. (b) The difference in the trajectories of the circular motion of skyrmions in PMA films with or without an IMA edge.

area of the circular trajectories becomes larger as a increases. However, the trajectories for different a have a similar shape. The T increases almost linearly from about 3 ns to 9 ns as a changes from 80 nm to 140 nm [Fig. 3(b)]. This result indicates that the period of the skyrmion-based signal generator can be tuned simply by changing the film size.

The dependencies of J_d, K_u, and D on the trajectory and T are depicted in Fig. 4. The diameter d, as indicated in Fig. 4(a), increases with increasing D [inset of Fig. 4(a)]. To generate a skyrmion with a smaller (larger) D, K_u also needs to be smaller (larger). The initial distances from the core of the skyrmion to the boundaries of the two sides are denoted by Δx and Δy ($\Delta x = \Delta y$) [Fig. 4(a)]. We note that a change in J_d results in a variation in the distance between the starting and ending points on the diagonal in the half-period. Therefore, to ensure the centrosymmetry, the starting point needs to be shifted along the diagonal and be closer to the edge for a higher J_d and a smaller D [Fig. 4(b)]. The representative circular trajectories are shown in Fig. 4(c). T decreases as J_d or D increases, as shown in Fig. 4(d). With an increase in J_d, the trajectory expands, but T decreases, indicating that the increase in J_d results in a significant increase in v. However, the trajectory shrinks with the increase in D, which simultaneously reduces T.

In addition to single PMA films, we also propose a composite structure consisting of a square film with PMA center areas and an in-plane magnetic anisotropy (IMA) edge. This design can be realized using experimental techniques such as Ar^+ ion milling or oxidation.[29,30] As shown in Fig. 5(a), four IMA regions ($K_u = 0.8 \times 10^4$ J/m^3) with lengths of 50 nm and widths of 10 nm are distributed on the four sides of a square-shaped film having a width of 100 nm and have centrosymmetry. The direction of moments in the IMA regions is opposite to that of the perimeter of the skyrmion. In this way, the path of motion is compressed, as shown in Fig. 5(b). As a result, T is reduced from 5.0 ns to 3.3 ns compared with a film with no IMA regions.

From Figs. 4(c) and 5(b), one can see that the area and the shape of the trajectory of the skyrmion are affected by changing K_u and D. In a PMA film with confined geometry, tilting moments exist near the edge. The spatial variation of moment orientation near the edge, which acts on a nearby skyrmion as an edge force, relies on K_u and D.[23] The mechanism of edge force is depicted in detail in the supplementary material (S2). Additionally, the formation of defects in a film is unavoidable. Moments with spatially varied orientation locate around a defect. As a result, a skyrmion feels a force when it moves close to the defect, and its trajectory is modified. However, if only the distribution of defects is random or exhibits centrosymmetry like the IMA edges in Fig. 5, the trajectory is still a closed loop and its symmetry is kept.

In summary, we proposed a skyrmion-based high-frequency signal generator via the SOT-driven circular motion of a skyrmion in a square-shaped magnetic thin film. Via the use of a pulsed current, a skyrmion moves on a closed curve with central symmetry. The starting point needs to shift, and the cycle period T can be adjusted by tuning parameters including the size of the square film, the current density, the magnetic anisotropy constant, and the DMI constant. In our simulation, T can vary from less than several nanoseconds to tens of nanoseconds or larger. Moreover, we proposed a composite structure consisting of a PMA square film with an IMA edge, which can change the trajectory of circular motion and reduce T.

See supplementary material for the principle for the detection of a skyrmion by a magnetic tunnel junction (MTJ) (S1) and the principle for the force acting on a skyrmion from the edge of a square-shaped film (S2).

This work was supported by the National Natural Science Foundation of China [Grant Nos. 11574096 and 61674062].

[1]S. Mühlbauer, B. Binz, F. Jonietz, C. Pfleiderer, A. Rosch, A. Neubauer, R. Georgii, and P. Böni, Science **323**, 915 (2009).
[2]X. Z. Yu, Y. Onose, N. Kanazawa, J. H. Park, J. H. Han, Y. Matsui, N. Nagaosa, and Y. Tokura, Nature **465**, 901 (2010).
[3]S. Heinze, K. von Bergmann, M. Menzel, J. Brede, A. Kubetzka, R. Wiesendanger, G. Bihlmayer, and S. Blügel, Nat. Phys. **7**, 713 (2011).
[4]X. Z. Yu, N. Kanazawa, Y. Onose, K. Kimoto, W. Z. Zhang, S. Ishiwata, Y. Matsui, and Y. Tokura, Nat. Mater. **10**, 106 (2011).
[5]J. Sampaio, V. Cros, S. Rohart, A. Thiaville, and A. Fert, Nat. Nanotechnol. **8**, 839 (2013).
[6]A. Fert, V. Cros, and J. Sampaio, Nat. Nanotechnol. **8**, 152 (2013).
[7]N. Nagaosa and Y. Tokura, Nat. Nanotechnol. **8**, 899 (2013).
[8]W. Kang, Y. Huang, X. Zhang, Y. Zhou, and W. Zhao, Proc. IEEE **104**, 2040 (2016).
[9]G. Finocchio, F. Büttner, R. Tomasello, M. Carpentieri, and M. Kläui, J. Phys. D: Appl. Phys. **49**, 423001 (2016).
[10]X. Zhang, Y. Zhou, M. Ezawa, G. P. Zhao, and W. Zhao, Sci. Rep. **5**, 11369 (2015).
[11]X. Zhang, M. Ezawa, and Y. Zhou, Sci. Rep. **5**, 9400 (2015).
[12]S. Zhang, J. Wang, Q. Zheng, Q. Zhu, X. Liu, S. Chen, C. Jin, Q. Liu, C. Jia, and D. Xue, New J. Phys. **17**, 023061 (2015).
[13]W. Jiang, P. Upadhyaya, W. Zhang, G. Yu, M. B. Jungfleisch, F. Y. Fradin, J. E. Pearson, Y. Tserkovnyak, K. L. Wang, O. Heinonen, S. G. E. te Velthuis, and A. Hoffmann, Science **349**, 283 (2015).
[14]A. A. Thiele, Phys. Rev. Lett. **30**, 230 (1973).

[15]M. Stone, Phys. Rev. B **53**, 16573 (1996).
[16]J. Zang, M. Mostovoy, J. H. Han, and N. Nagaosa, Phys. Rev. Lett. **107**, 136804 (2011).
[17]W. Jiang, X. Zhang, G. Yu, W. Zhang, X. Wang, M. B. Jungfleisch, J. E. Pearson, X. Cheng, O. Heinonen, K. L. Wang, Y. Zhou, A. Hoffmann, and S. G. E. te Velthuis, Nat. Phys. **13**, 162 (2017).
[18]J. Iwasaki, M. Mochizuki, and N. Nagaosa, Nat. Nanotechnol. **8**, 742 (2013).
[19]R. Tomasello, E. Martinez, R. Zivieri, L. Torres, M. Carpentieri, and G. Finocchio, Sci. Rep. **4**, 6784 (2014).
[20]X. Zhang, M. Ezawa, D. Xiao, G. P. Zhao, Y. Liu, and Y. Zhou, Nanotechnology **26**, 225701 (2015).
[21]I. Purnama, W. L. Gan, D. W. Wong, and W. S. Lew, Sci. Rep. **5**, 10620 (2015).
[22]N. Romming, C. Hanneken, M. Menzel, J. E. Bickel, B. Wolter, K. von Bergmann, A. Kubetzka, and R. Wiesendanger, Science **341**, 636 (2013).
[23]S. Rohart and A. Thiaville, Phys. Rev. B **88**, 184422 (2013).
[24]J. Sinova, S. O. Valenzuela, J. Wunderlich, C. H. Back, and T. Jungwirth, Rev. Mod. Phys. **87**, 1213 (2015).
[25]H. Yang, A. Thiaville, S. Rohart, A. Fert, and M. Chshiev, Phys. Rev. Lett. **115**, 267210 (2015).
[26]Y. Zhou and M. Ezawa, Nat. Commun. **5**, 4652 (2014).
[27]J. C. Martinez and M. B. A. Jalil, J. Magn. Magn. Mater. **424**, 291 (2017).
[28]SH. Sato, S. Ikeda, S. Fukami, H. Honjo, S. Ishikawa, M. Yamanouchi, K. Mizunuma, F. Matsukura, and H. Ohno, Jpn. J. Appl. Phys., Part 1 **53**, 04EM02 (2014).
[29]L. You, O. Lee, D. Bhowmik, D. Labanowski, J. Hong, J. Bokor, and S. Salahuddin, Proc. Natl. Acad. Sci. U. S. A. **112**, 10310 (2015).
[30]G. Yu, P. Upadhyaya, Y. Fan, J. G. Alzate, W. Jiang, K. L. Wong, S. Takei, S. A. Bender, L. T. Chang, Y. Jiang, M. Lang, J. Tang, Y. Wang, Y. Tserkovnyak, P. K. Amiri, and K. L. Wang, Nat. Nanotechnol. **9**, 548 (2014).